MODELING OF A BUOYANCY-DRIVEN FLOW EXPERIMENT IN PRESSURIZED WATER REACTORS USING CFD-METHODS

THOMAS HÖHNE* and SÖREN KLIEM
Forschungszentrum Dresden-Rossendorf(FZD) - Institute of Safety Research,
P.O. Box 510119 01314 Dresden, Germany
*Corresponding author. E-mail : T.Hoehne@fzd.de

Received March 28, 2007
Accepted for Publication June 12, 2007

The influence of density differences on the mixing of the primary loop inventory and the Emergency Core Cooling (ECC) water in the downcomer of a Pressurised Water Reactor (PWR) was analyzed at the ROssendorf COolant Mixing (ROCOM) test facility. ROCOM is a 1:5 scaled model of a German PWR, and has been designed for coolant mixing studies. It is equipped with advanced instrumentation, which delivers high-resolution information for temperature or boron concentration fields. This paper presents a ROCOM experiment in which water with higher density was injected into a cold leg of the reactor model. Wire-mesh sensors measuring the tracer concentration were installed in the cold leg and upper and lower part of the downcomer. The experiment was run with 5 % of the design flow rate in one loop and 10 % density difference between the ECC and loop water especially for the validation of the Computational Fluid Dynamics (CFD) software ANSYS CFX. A mesh with two million control volumes was used for the calculations. The effects of turbulence on the mean flow were modelled with a Reynolds stress turbulence model. The results of the experiment and of the numerical calculations show that mixing is dominated by buoyancy effects: At higher mass flow rates (close to nominal conditions) the injected slug propagates in the circumferential direction around the core barrel. Buoyancy effects reduce this circumferential propagation. Therefore, density effects play an important role during natural convection with ECC injection in PWRs. ANSYS CFX was able to predict the observed flow patterns and mixing phenomena quite well.

KEYWORDS : CFD, ROCOM, Coolant Mixing, RPV, PWR

1. INTRODUCTION

Density differences between the coolant water and the primary loop inventory can play an important role during loss-of-coolant accidents in nuclear power plants, as the injection of the relatively cold Emergency Core Cooling (ECC) water can induce buoyancy-driven stratification. This stratification can cause high temperature gradients and increased thermal stresses of the Reactor Pressure Vessel (RPV) and these scenarios are called pressured thermal shocks (PTS) scenarios. Moreover, in case of inadvertent injection of ECC water with low boron concentration, a boron dilution transient could be initiated. Grundmann [1] has shown that the assumption of a homogeneous distribution (i.e. ideal mixing) of the injected lower borated water at the core inlet of Pressurized Water Reactors (PWR) does not yield conservative results. The remaining uncertainties are much too large to be acceptable for safety analyses: There are for instance numerous postulated accident scenarios in which the reactor core would survive undamaged or would not even reach criticality under the assumption of ideal mixing, whereas incomplete mixing would lead to fuel rod failures. In reality, partial mixing takes place, and the detailed mixing pattern at the core inlet is required to make accurate and realistic predictions about the safety of the reactor. This mixing pattern is the consequence of a complex three-dimensional fluid flow. Recent progress in computer hardware and numerical techniques has made it viable to predict these mixing patterns using CFD codes, see for instance the contributions by Alvarez [2], Alavyoon [3], and Höhne ([4], [5], [6]). However, as CFD codes contain more or less empirical models (for instance turbulence models), it is necessary to validate the predicted results using experimental data. This is especially important in case of safety-critical coolant mixing phenomena. There are several test facilities to study mixing of cold ECC water injected into the cold leg of a

PWR, see [7], [8], [9] and [10]. In order to examine coolant mixing in the RPV of a German-type PWR, the Rossendorf COolant Mixing Model (ROCOM) test facility was used in the current work. ROCOM is a 1:5 scaled KONVOI-type PWR (1,300 MW_{el}). Data obtained for an experiment with a constant flow rate in one loop (magnitude of natural circulation) and 10 % density difference between the ECC and loop water were compared with predictions obtained from the CFD software ANSYS CFX.

2. ROCOM TEST FACILITY

The ROCOM test facility [4] consists of a RPV model (Fig. 1) with four inlet and four outlet nozzles. The facility is equipped with four fully operating loops (Fig. 2), i.e. it has four circulation pumps, which are driven by motors with computer-controlled frequency transformers. As a result, a wide variety of operating regimes, such as four-loop operation, operation with pumps off, simulated natural circulation modes and flow rate ramps can be realized. For natural circulation investigations, the pumps are operated at low speed by means of the frequency transformer system. Geometric similarity between the original reactor and ROCOM is maintained from the inlet nozzles to the core inlet. The core itself is excluded from the similarity; rather, a core simulator with the same Euler number (pressure drop vs. flow head) as in the original reactor is used. The ROCOM reactor model is manufactured from Plexiglas® (Fig. 1). The reactor model describes the geometry of the original PWR with respect to the design of the nozzles (diameter, curvature radii, and diffuser parts), the character-istic extension of the downcomer cross section below the nozzle zone, the perforated drum in the lower plenum and the design of the core support plate with the orifices for the coolant. The flow rate in the loops is scaled according to the transit time of the coolant through the reactor model. Since the geometrical scale of the facility is 1:5, the transit time of the coolant becomes identical to the original reactor when the coolant flow rate is also scaled by 1:5.

From these scaling laws, the nominal flow rate in ROCOM was set to 185 m^3/h per loop. The Reynolds numbers in ROCOM are approximately two orders of magnitude smaller than in the original. A factor of 25 results from the down-scaling of the geometry and the mass flow rates (velocities). The remaining difference comes from operation at room temperature and ambient pressure. At room temperature, the viscosity of water is approximately by a factor of 8 higher than for original reactor conditions.

Since coolant mixing is mainly caused by turbulent dispersion (which is independent of the exact fluid properties) it is possible to use a tracer substance to model differences of boron concentration or coolant temperature. The coolant in the disturbed loop was marked by injecting a sodium chloride solution into the main coolant flow upstream of the reactor inlet nozzle. Magnetic valves controlled the injection process. As the ROCOM facility can not be heated, the higher density of the cold ECC water was simulated by adding sugar (glucose). In the current experiment a density difference of 10 % was used. A sugar solution with a corresponding density of 1,100 kg/m^3 has a viscosity, which is by factor of 3 higher than that of pure water. The sugar tracer can therefore still be envisaged as a fluid with low viscosity.

Fig. 1. Reactor Model of the ROCOM Test Facility

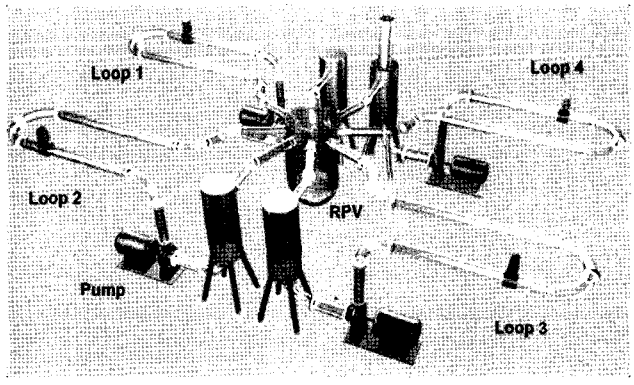

Fig. 2. ROCOM Test Facility with Four Loops and Individual Frequency Controlled Circulation Pumps

3. INSTRUMENTATION

The tracer distribution in the reactor model was measured by electrode-mesh sensors [11], which sample the distribution of the electrical conductivity over the cross section of the flow path. Two perpendicular grids of electrodes insulated from each other are placed across the flow duct. The electrodes of the first grid (transmitter electrodes) are successively charged with short voltage pulses. The currents arriving at the electrodes of the second grid are recorded (receiver electrodes). After a complete cycle of transmitter activation a complete matrix of local conductivities is obtained.

The wire mesh sensors are placed at four positions of the flow path. The first sensor is flanged to the reactor inlet nozzle (Fig. 3) in cold leg 1. It observes the distribution at the reactor inlet. The second and the third sensor are located at the upper and at the lower downcomer (Fig. 3). The downcomer sensors consist of 64 radial fixing rods with orifices for four circular electrode wires. Small ceramic insulation beads separate rods and wires electrically. The rods are acting as radial electrodes, i.e. each rod corresponds to a circumferential measuring position.

Approximately 1,000 measuring points are recorded in total. The measuring frequency is 200 Hz. In most cases 10 successive measure-ments were averaged and the result was stored with a frequency of 20 Hz, because the characteristic frequency of the observed phenomena did not require a higher sampling frequency. The measured local conductivities are then related to reference values. The result is a mixing scalar which characterizes the instantaneous share of coolant originating from the disturbed loop (i.e. where the tracer is injected) at a given location inside the flow field. This scalar is dimensionless. Assuming similarity between the tracer field and the temperature and boron concentration fields, it can be used to apply the experimental results to the original reactor. The reference values correspond to the unaffected coolant (index '0') and the coolant at the disturbed reactor inlet nozzle (index '1'). The difference between the two reference values is the magnitude of the perturbation. The mixing scalar θ is defined as follows:

$$\theta_{x,y,z,t} = \frac{\sigma_{x,y,z,t} - \sigma_0}{\sigma_1 - \sigma_0} \cong \frac{T_{x,y,z,t} - T_0}{T_1 - T_0} \cong \frac{C_{B,x,y,z,t} - C_{B,0}}{C_{B,1} - C_{B,0}} \quad (1)$$

Here, σ is the electrical conductivity, T is the temperature and C_B the boron concentration. Which of the two parameters temperature or boron concentration is represented by the measured mixing scalar depends on the correct choice of the reference values and the setup of

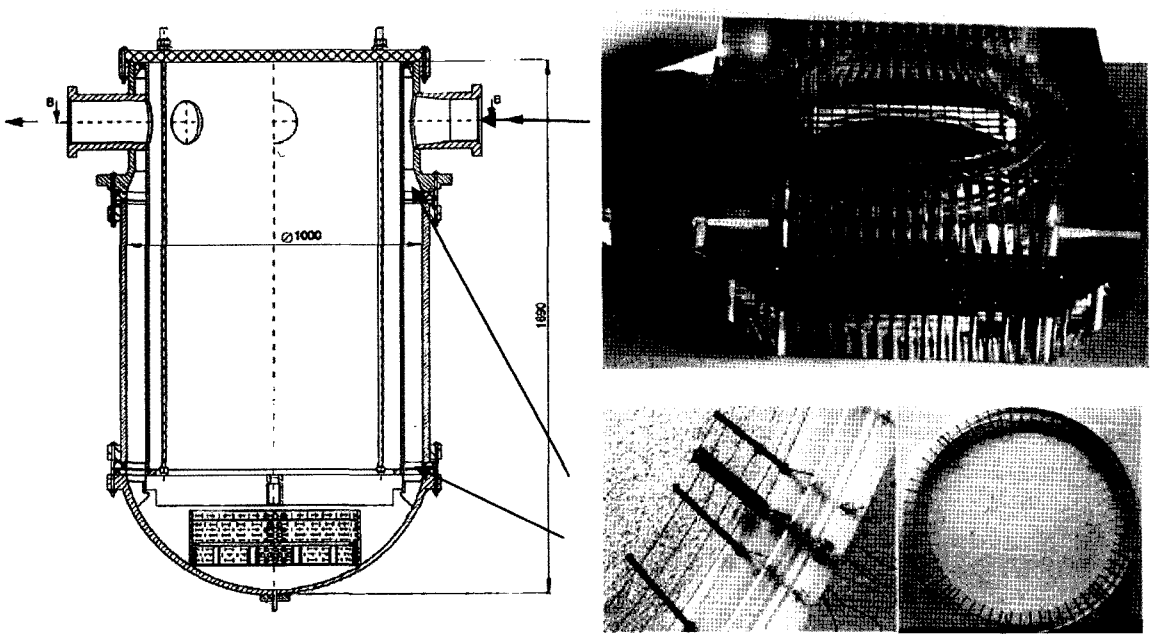

Fig. 3. Sensor Positions in the RPV

the boundary conditions in the experiment. Linearity between the tracer concentration and the measured local conductivity is used to transform the conductivity measurements of the wiremesh sensor into dimensionless scalar concentrations. However, the addition of sugar changes the linear relation between tracer concentration and conductivity. Therefore, the original correlation for solutions at low viscosity was replaced by a function, which depends also on the normalized viscosity, which is proportional to the density of the glucose-water mixture.

4. ECC WATER INJECTION WITH DENSITY EFFECTS

The objective of the experiments was the investigation of the effects of density differences between the primary loop inventory and the ECC water on the mixing in the downcomer. The mass flow rate was varied between 0 and 15 % of the nominal flow rate, i.e. it was kept at the same order of magnitude as the natu-ral circulation. The density differences between ECC and loop water were varied between 0 and 10 %. Fig. 4 summarizes the boundary conditions of the experiments.

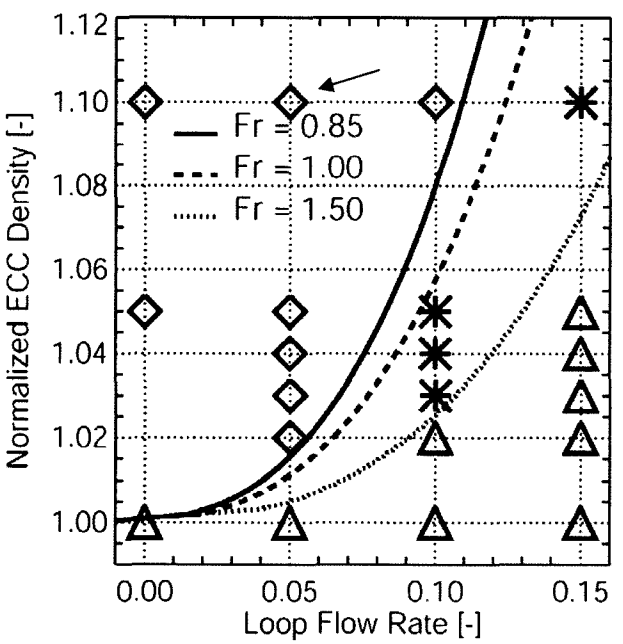

Fig. 4. Test Matrix of ECC Injection Experiments, Classification of the ROCOM Tests, Isolines of Froude Numbers

In total, 21 experiments were carried out (signs in Fig. 4). The analysis of all experiments is presented in [17]. In that paper, a criterion for the distinction between momentum driven and density driven flow based on the experimental data has been developed. In order to find this criterion, generic density differences were used, which do not always correspond to conditions under hypothetical accident scenarios of the prototype reactor. The set of experiments shown in Figure 4 was divided into three groups: Density dominated flows (◇), momentum-dominated flows (Δ) and the transition region (*). The conditions at the inlet into the downcomer were used to calculate Froude numbers, defined by:

$$Fr = \frac{v_{in}}{\sqrt{g \cdot s \cdot \frac{\rho_{in} - \rho_a}{\rho_{in}}}} \qquad (2)$$

v_{in} is the velocity at the reactor inlet (combined loop and ECC flow), g is the gravitational acceleration, s is the length of the downcomer, ρ_{in} the density of the incoming flow, calculated with the assumption of homogeneous mixing between ECC and loop flow, and ρ_a the density of the ambient water in the downcomer. The lines of constant Froude numbers calculated by Eq. (2) are shown in Fig. 4.

All density-dominated experiments are located to the left of the iso-line Fr = 0.85 and all momentum-dominated experiments are located to the right of the iso-line Fr = 1.50. These two numbers are critical Froude numbers separating the two flow regimes for the ROCOM test facility. The transition region is located between these two values.

From the whole set of data the experiment with 5 % constant flow rate in one loop and 10 % density difference between ECC and loop water was selected for the calculations (Table 1). The Froude number is Fr = 0.366. It is labelled as density-dominated (in Fig. 3 on the upper left side) and therefore suitable for analysing buoyancy effects.

5. NUMERICAL MODELING WITH ANSYS CFX

The CFD code for simulating the mixing studies was ANSYS CFX [13]. ANSYS CFX is an element-based finite-volume method with second-order discretisation schemes in space and time. It uses a coupled algebraic multigrid algorithm to solve the linear systems arising from discretisation. The discretisation schemes and the multigrid solver are scalably parallelized. ANSYS CFX works with unstructured hybrid grids consisting of tetrahedral, hexahedral, prism and pyramid elements.

5.1 Numerical Scheme, Nodalization, Time Step Size and Turbulence Modelling

The overall error of a CFD calculation is a combination

Table 1. Experiment Chosen for Code Validation

$\dot{V}$ (ECC) / m³/h	$\dot{V}$ (n°1) / m³/h	Density difference Loop / ECC water	Fr (Downcomer)
3.6	9.25	1:1.1	0.366

of several aspects: Grid density, discretisation method, time step size, iteration error and the employed mathematical models have all their own effect. The separation of these error components for complex three-dimensional calculation is difficult. For example discretisation errors can act like an additional numerical diffusivity, and can affect the results in a similar way as too large eddy viscosity arising from an unsuitable turbulence model.

Discretisation errors can be reduced by using finer grids, higher-order discretisation methods and smaller time step sizes. However, in many practical three-dimensional applications grid- and time step-independent solutions cannot be obtained because of hardware limitations. In these cases, the remaining errors and uncertainties should be quantified as described in the ECORA Best Practice Guidelines (BPG) by Menter [14]. In the current study, the CFD simulations were performed according to these BPGs. A convergence criterion of 1×10^{-5} was used to ensure negligibly small iteration errors. Round-off errors were quantified by comparing results obtained with single and double precision versions of the code. No differences were observed. In the calculations shown below, the High-Resolution (HR) discretisation scheme of ANSYS CFX was used to discretise the convective terms in the model equations. A second-order implicit scheme was used to approximate the transient terms. The used time step size was 0.05 s. The glucose water, which had a higher density, was modelled with the multi-component model of ANSYS CFX. In a multi-component flow, the components share the same velocity, pressure and temperature fields. The properties of multi-component fluids are calculated on the assumption that the constituent components form an ideal mixture. The glucose water is modelled as a component with different density and viscosity compared to water. The mass fraction of the glucose water can be directly related to the mixing scalar described in Eq. (1). The Reynolds stress model (RSM) proposed by Launder et al. [15], which is based on the Reynolds Averaged Navier-Stokes Equations (RANS), was used in combination with an ω-based length scale equation (BSL model) to model the effects of turbulence on the mean flow. Buoyancy production terms were included in the Reynolds stress equations and in the length-scale equation. The buoyancy production terms in the Reynolds stress equations are exact terms and require no modelling. A transient of 50 s was simulated. The calculations were performed on 6 processors of a LINUX cluster (dual CPU compute nodes, XEON, 3.2 GHz, ~1.3 Gflops, each containing 2GB RAM) and they took 2 weeks to complete.

5.2 Geometrical Simplifications, Local Details

The geometric details of the ROCOM internals have a strong influence on the flow field and on the mixing. Therefore, an exact representation of the inlet region, the downcomer below the inlet region, and the obstruction of the flow by the outlet nozzles in the downcomer is necessary (see Figs. 5 and 6). In the current study, these geometric details were modelled using the ICEM CFD

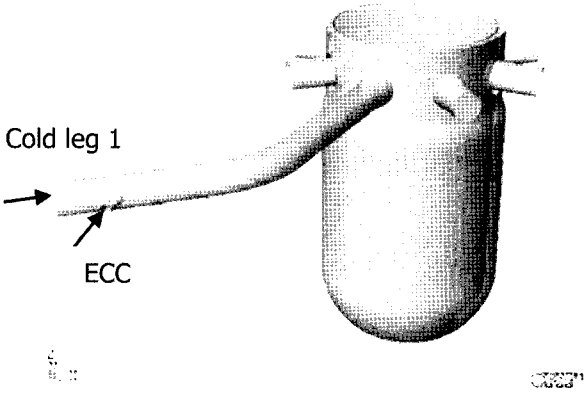

Fig. 5. Flow Domain with Inlet Boundary Conditions

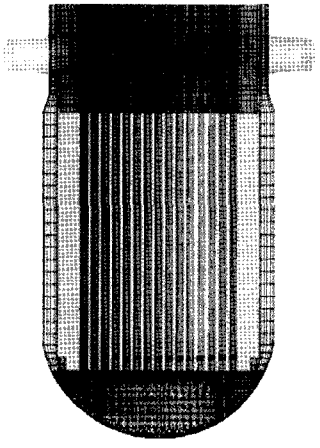

Fig. 6. Hybrid Mesh Vertical Cut

software. The final model included the inlet nozzles with the diffuser part, the orifices of the outlet nozzles, the downcomer extension, the lower plenum, the core support plate, the perforated drum, the core simulator, the upper plenum, and the outlet nozzles. Then the fluid flows through the hydraulic core simulator inside the tubes shown in Fig. 6. The perforated drum contains 410 orifices of 15 mm diameter.

5.3 Grid Generation

The mesh was generated with the ICEM CFD software. It consisted of 2 million nodes and 4 million hybrid elements (Figs. 5 and 6). The mesh was refined at the perforated drum, in the lower support plate and at the ECC injection line. The downcomer and nozzle region was discretized with hexahedral cells; tetrahedral elements were used for the lower plenum (Fig. 6).

6. BOUNDARY AND INITIAL CONDITIONS

Inlet boundary conditions were specified at the ECC injection line and after the knee of the cold leg 1. A uniform velocity distribution was used to simulate the one ECC injection for 10 sec, as shown in Fig. 7. A uniform velocity profile was also defined at the ECC injection line. At all other times the ECC injection velocities was set to zero. The mixing scalar of the glucose water was set to 1 at the ECC injection line and to 0 at the inlet of cold leg 1, as shown in Fig. 8.

A constant static pressure was specified at the outlet nozzles. A no-slip boundary condition with automatic linear/logarithmic wall functions was used at all solid walls. The initial velocity field was set to 5 % of the nominal flow (9.25 m^3/h) in cold leg 1. The velocities in the idle loops were defined as zero.

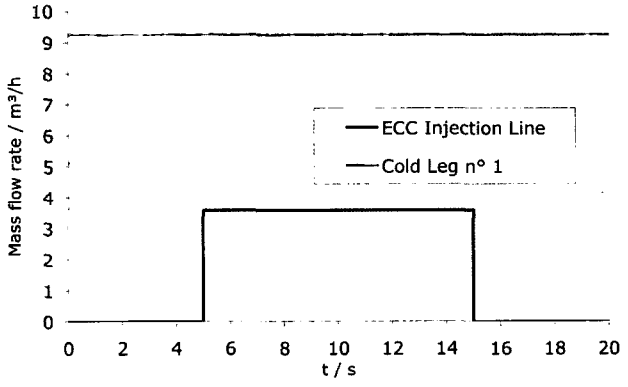

Fig. 7. Mass Flow Rate Over Time (Cold Leg 1, ECC Injection)

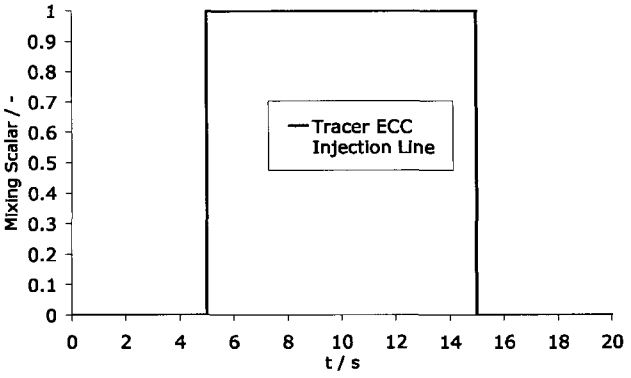

Fig. 8. Mixing Scalar of Glucose Water Over Time at the ECC Injection Line

7. RESULTS

7.1 Experimental Findings

Figure 9 shows the time evolution of the tracer concentration measured at the two downcomer sensors in an unwrapped view.

The second arrow from left at the top indicates the position of the loop with the running pump, delivering 5 % of the nominal mass flow rate. The density difference between the injected ECC water and the primary loop coolant is 10 %. At the upper downcomer sensor, the ECC water (injected in the experiment from t = 5 to t = 15 s) appears directly below the inlet nozzle. At the outset the area wetted by the ECC water is bigger below the inlet nozzle, because the momentum driven flow field is still dominant. Thereafter the density differences suppress the propagation of the ECC water in the circumferential direction. The ECC water falls down in an almost straight line and reaches the lower downcomer sensor directly below the inlet nozzle. Only at later times does ECC water appear at the opposite side of the downcomer. The maximum concentration values observed at the two downcomer sensors are 39.1 % and 14.0 % of the initial concentration in the ECC water tank (Fig 10).

7.2 Qualitative Analysis of the CFD Calculation

The first part of the transient calculation was used to establish a flow field in the cold leg and downcomer of ROCOM. During this period the ECC injection line was closed. The ensuing flow in cold leg 1 creates a momentum-controlled flow entering the downcomer. It is divided into two jets flowing in a downwards-directed helix around the core barrel (Figure 11). A similar behaviour was observed during nominal flow conditions using one pump in [17]. After the onset of the injection, the flow

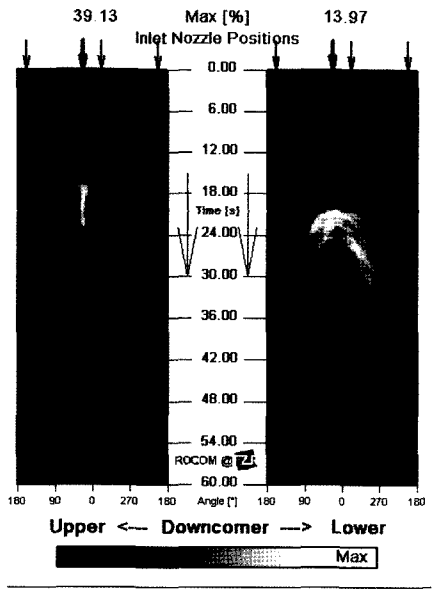

Fig. 9. Time Dependent Tracer Distributions at the Upper and Lower Downcomer Sensor

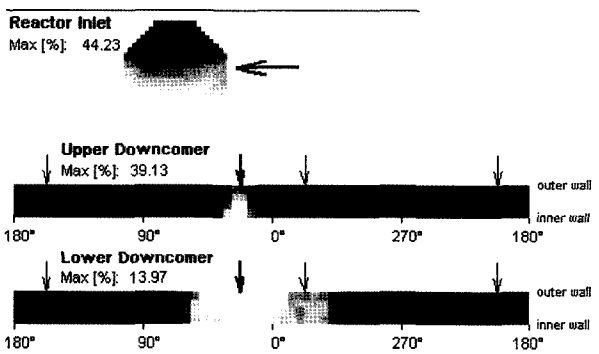

Fig. 10. Time Dependent Tracer Distributions at the Cold Leg 1, Upper and Lower Downcomer Sensor at 23 s Simulation Time

pattern in the cold leg changes because of buoyancy effects. The cold water from the ECC injection line first hits the opposite wall of cold leg 1; this is caused by the momentum of the injected jet (Figure 12). Later, the ECC water is partly mixing with the ambient loop inventory, but mainly propagating towards the reactor inlet at the bottom of the cold leg. During the period of injection and after completion of the injection, the cold leg flow transports the ECC water towards the reactor inlet. As in the experiments, the area covered by the ECC water is bigger below the inlet nozzle, because the momentum-driven flow field is still present (Figure 13). However, because of the density differences between the ECC water and the ambient coolant, the initial momentum-controlled flow in the downcomer starts changing. At later times a density-dominated flow is established (Figs. 12 and 14). The heavier ECC water creates a downward streak in the downcomer. During this downward flow, the ECC water in the downcomer is well mixed with the ambient coolant. When the streak reaches the lower plenum, it swaps to the opposite side of the injection loop. By this time the lower plenum is filled with already well-mixed ECC water.

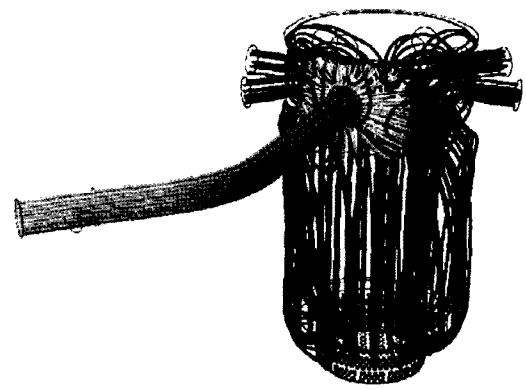

Fig. 11. Streamlines Representing the Fluid Flow Before the Injection Takes Place (4 s)

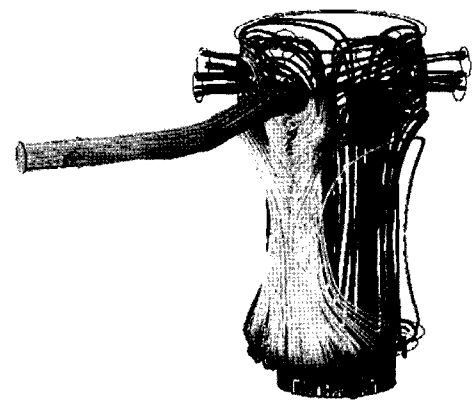

Fig. 12. Streamlines Representing the Fluid Flow After the Injection Took Place (23 s)

7.3 Quantitative analysis of the CFD calculation

At the cold leg sensor 216 measurement points (Figs.

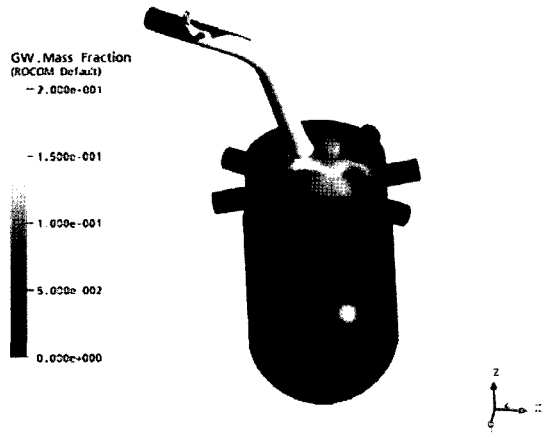

Fig. 13. Tracer Distribution (16 s)
Zoomed Mixing Scalar θ (0.0-0.2)

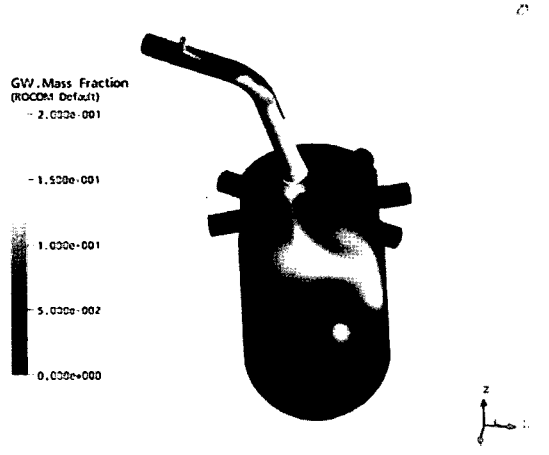

Fig. 14. Tracer Distribution in the Downcomer (21 s)
Zoomed Mixing Scalar θ (0.0-0.2)

15 and 16) and 32 circumferential sensor positions in the middle of the upper and lower downcomer sensor plane were selected (Figs. 17-20) for comparison of experimental data and numerical predictions. A local position in the downcomer region below the inlet nozzle cold leg 1 was selected for comparison of the experiment and the calculation shown in Figs. 17 and 19.

The transient slug behaviour is plotted at a local position in the centre of the sensor in Figure 15. At the position 0312 the predicted mixing scalar θ agrees well with the experimental values. Figure 16 shows the circumferential distribution of the slug at the outer wall of the cold leg sensor. The 0°-position is at the bottom of the cold leg.

The calculations reflect the observed stratification of the experiment. At a circumferential angle of 42.5° (Figure 17) the mixing scalar θ achieved values similar to the experiment (maximum $\theta_{local} = 0.24$), however at a different time in the upper downcomer sensor. The difference to the experimental values at the maximum is 2%. The circumferential distribution of the mixing scalar θ at 21 s shown in Figure 18 shows the creation of a downwards streak in the downcomer below the inlet nozzle of cold leg 1. The shape of the perturbation is almost identical. In the lower downcomer the maximum values of the mixing scalar are smaller than in the upper downcomer part (Figure 19). In the 42.5°-position (Figure 19) the mixing scalar θ is almost reaching the values of the experiment (maximum $\theta_{local} = 0.13$). However, the peak for the numerical trace is slightly earlier than the experimental values. Also, a larger area below cold leg 1 and cold leg 2 is covered by the slug in the lower downcomer position (Figure 20).

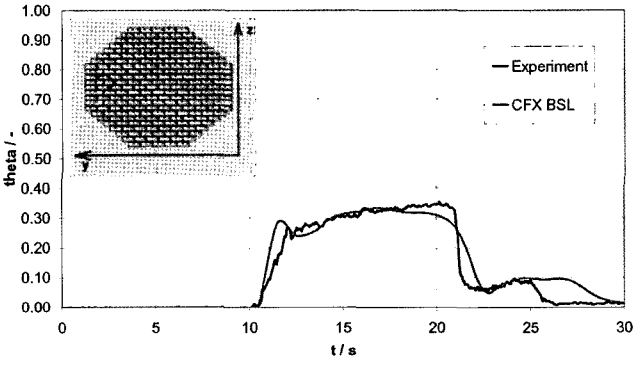

Fig. 15. Time Dependent Tracer Distribution at the Cold Leg Sensor (Local Position 0312)

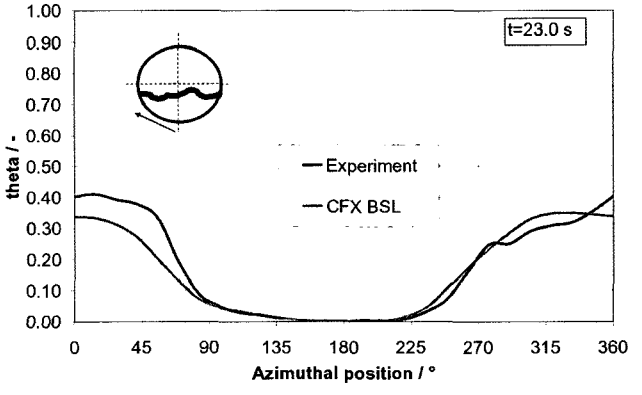

Fig. 16. Time Dependent Tracer Distribution at Cold Leg Sensor (Circumferential Position, 23 s)

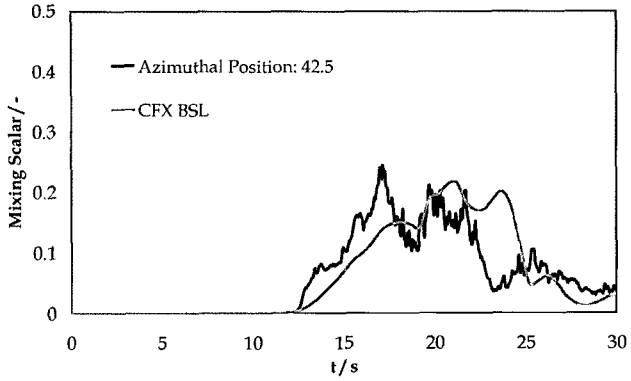

Fig. 17. Tracer Distribution at Circumferential Position 42.5° of the Upper Downcomer

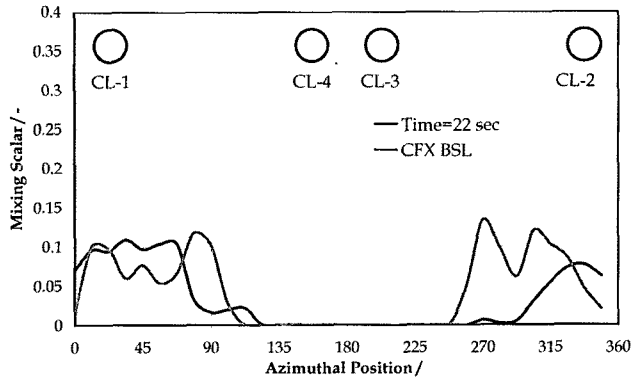

Fig. 20. Tracer Distribution in the Unwrapped Lower Downcomer (22 s)

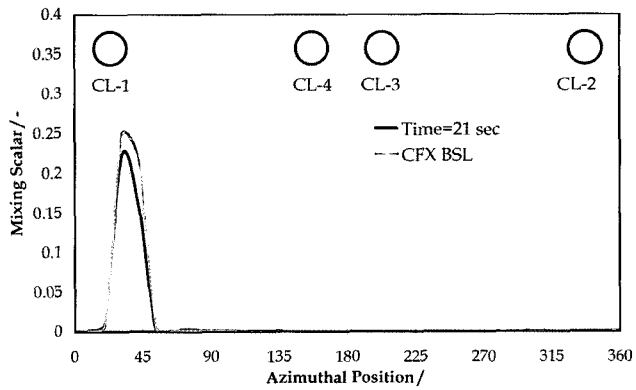

Fig. 18. Tracer Distribution in the Unwrapped Upper Downcomer (21 s)

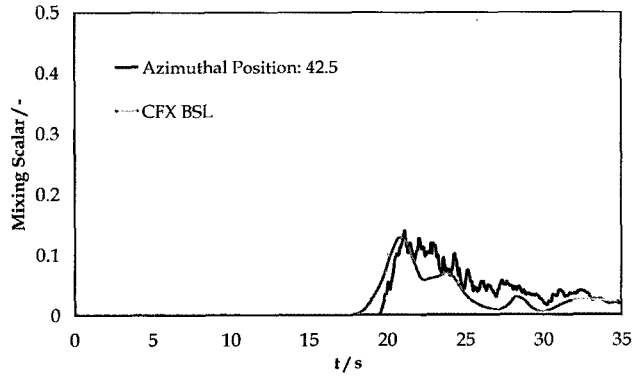

Fig. 19. Tracer Distribution at Circumferential Position 42.5° of the Lower Downcomer

8. SUMMARY

A ROCOM experiment with constant flow rate in one loop (magnitude of natural circulation) and 10 % density difference between ECC and loop water was used to validate the CFD software ANSYS CFX. A Reynolds stress turbulence model was employed to model the effects of turbulence on the mean flow. A hybrid mesh consisting of 2 million nodes and 4 million elements was used. The calculations predict the experimentally observed behaviour that the ECC water partly mixes only with the ambient loop inventory in the cold leg. A stratified flow is developing during the injection. In the downcomer, a momentum-driven flow field is present at the start of the injection. At later times, the flow becomes density dominated, and the ECC water propagates vertically downwards in the downcomer. The ANSYS CFX calculations show a good qualitative agreement with the experimental data. At some local positions differences in the predicted and measured concentration fields occur. To improve the agreement of the CFD calculation with measured data, advanced turbulence models using for instance a DES (Detached Eddy Simulation) approach should be utilized.

ACKNOWLEDGMENTS

The project this paper is based on was partly funded by EC under contract FIKS-CT-2001-00197.

REFERENCES

[1] U. Grundmann, U. Rohde. Investigations on a boron dilution accident for a VVER-440 type reactor by the help of the code DYN3D. ANS Topical Meeting on Advances in Reactor Physics, Knoxville, TN. April 11-15, vol. 3, pp. 464-471, 1994.

[2] D. Alvarez et al. Three dimensional calculations and experimental investigations of the primary coolant flow in

a 900 MW PWR vessel. Proc. NURETH-5, vol. II, pp. 586-592, 1992.

[3] F. Alavyoon, B. Hemström, N.G. Andersson, R. Karlsson. Experimental and computational approach to investigating rapid boron dilution transients in PWRs. CSNI Specialist Meeting on Boron Dilution Reactivity Transients, State College, Pennsylvania, USA, October 18-20, 1995.

[4] H.-M. Prasser, G. Grunwald, U. Rohde, S. Kliem, T. Höhne, R. Karlsson, F.-P. Weiss. Coolant mixing in a Pressurized Water Reactor: Deboration Transients, Steam-Line Breaks, and Emergency Core Cooling Injection. Nuclear Technology 143 (1), p.37, 2003.

[5] T. Höhne, Numerical Simulation of ISP-43 TEST A with CFX-4. Proceedings of 2002 ANS/ASME Student Conference. Penn State University, CD-ROM, 2002.

[6] T. Höhne, Grunwald G., Prasser H.-M. Investigation of coolant mixing in Pressurized Water Reactors at the Rossendorf mixing test facility ROCOM. 8th International Conference on Nuclear Engineering, Baltimore, USA, CD-ROM, 2000.

[7] HDR safety program – thermal mixing in the cold leg and downcomer of the HDR test rig, Report PHDR 91-89. FZ Karlsruhe, Germany, 1990.

[8] K. Umminger, W. Kastner, J. Liebert, T. Mull. Thermal Hydraulics of PWR's with Respect to Boron Dilution Phenomena: Experimental Results from the Test Facilities PKL and UPTF. Ninth Int. Topical Meeting on Nuclear Reactor Thermal Hydraulics (NURETH–9), San Francisco, California, USA, CD-ROM, 1999.

[9] Y. A. Hassan, J. A. Randorf. Stratification Studies in Nuclear Reactor Components. NURETH-8, Kyoto, Japan, Vol 1, pp 449, 1997.

[10] B. Woods. UM 2x4 Loop Experimental Findings on the Effect of Inertial and Buoyancy forces on Annular Flow Mixing for Rapid Boron Dilution Transients. Ph.D. Thesis, University of Maryland, USA, 2001.

[11] T. Höhne, U. Bieder, H.-M. Prasser, S. Kliem. Validation of Trio_U – Numerical Simulations of a ROCOM Buoyancy Driven Test Case. 12th International Conference on Nuclear Engineering, Washington D.C., USA, April 25-29, Book of Abstracts, S. 278, 2004.

[12] H.-M. Prasser, A. Böttger, J. Zschau. A new electrode-mesh tomograph for gas-liquid flows. Flow Measurement and Instru-mentation 9. pp. 111-119, 2001.

[13] ANSYS CFX.-10 User Manual, ANSYS-CFX, 2005.

[14] F. Menter. CFD Best Practice Guidelines for CFD Code Validation for Reactor Safety Applications. ECORA FIKS-CT-2001-00154, 2002.

[15] Launder, B.E., Reece, G.J., Rodi, W. Progress in the development of a Reynolds-stress turbulence closure. J. Fluid Mech. 68 (3), 537–566, 1975.

[16] B. Hemström et al. Validation of CFD codes based on mixing experiments (Final report on WP4), EU/FP5 FLOMIX-R report, FLOMIX-R-D11. Vattenfall Utveckling (Sweden), 2005.

[17] Rohde, U.; Kliem, S.; Höhne, T.; Karlsson, R.; Hemström, B.; Lillington, J.; Toppila, T.; Elter, J.; Bezrukov, Y. Fluid mixing and flow distribution in the reactor circuit - Part 1: Measurement data base. Nuclear Engineering and Design 235, 421–443, 2005.